Composites Part B 111 (2017) 27–36

Contents lists available at ScienceDirect

Composites Part B

journal homepage: www.elsevier.com/locate/compositesb

Modeling the molecular structure of the carbon fiber/polymer interphase for multiscale analysis of composites

Joel P. Johnston*, Bonsung Koo, Nithya Subramanian, Aditi Chattopadhyay

School for Engineering of Matter, Transport, and Energy, Arizona State University, 551 East Tyler Mall, Tempe, AZ, USA

ARTICLE INFO

Article history:
Received 24 March 2016
Received in revised form
25 October 2016
Accepted 4 December 2016
Available online 7 December 2016

Keywords:
Polymer-matrix composites (PMCs)
Interface/interphase
Carbon fibre
Multiscale modelling

ABSTRACT

The carbon fiber/polymer matrix interphase region plays an important role in the behavior and failure initiation of polymer matrix composites and accurate modeling techniques are needed to study the effects of this complex region on the composite response. This paper presents a high fidelity multiscale modeling framework integrating a novel molecular interphase model for the analysis of polymer matrix composites. The interphase model, consisting of voids in multiple graphene layers, enables the physical entanglement between the polymer matrix and the carbon fiber surface. The voids in the graphene layers are generated by intentionally removing carbon atoms, which better represents the irregularity of the carbon fiber surface. The molecular dynamics method calculates the interphase mechanical properties at the nanoscale, which are integrated within a high fidelity micromechanics theory. Additionally, progressive damage and failure theories are used at different scales in the modeling framework to capture scale-dependent failure of the composite. Comparisons between the current molecular interphase model and existing interphase models and experiments demonstrate that the current model captures larger stress gradients across the material interphase. These large stress gradients increase the viscoplasticity and damage effects at the interphase which are necessary for improved prediction of the nonlinear response and multiscale damage in composite materials.

1. Introduction

Polymer composites, typically containing a polymer matrix and inorganic components (additives), are ubiquitous in industrial applications and daily life. The applications of polymer composites range from consumer products to structural materials. A major barrier limiting the applications of composites is a lack of confidence in the assessment of safety and reliability of these structures under service conditions. There is a need for accurate predictive tools that take into account constituent interactions, material and architectural variability, and damage at relevant length scales in order to capture the complex damage mechanisms and failure modes. A significant amount of research has been reported in this area. Voyiadjis et al. [1] developed a multiscale model including damage and plasticity variables at the meso- and macroscales. Yu and Fish [2] used asymptotic homogenization for the spatial and temporal domains to model viscoelastic behavior of composites. Bednarcyk and Arnold [3] incorporated stochastic fiber breakage phenomena within the Generalized Method of Cells (GMC) to study the tensile failure of unidirectional composite dogbone specimens. Liu et al. [4,5] developed a Multiscale Generalized Method of Cells (MSGMC) framework, which performed through-thickness homogenization, introducing normal/shear coupling, to study the material behavior and failure of composites with complex architectures. Macroscopic failure of composite structures was modeled using a multiscale progressive failure technique by Laurin et al. [6]. Ghosh et al. [7,8] developed a multiscale Voronoi cell finite element approach using random microstructure to analyze composite failure. Borkowski et al. [9] studied the effect of microstructural randomness on polymer matrix composite (PMC) properties using finite element analysis (FEA). However, these modeling studies assume perfect bonding conditions for the fiber/polymer matrix interphase; whereas the physical structure and interactions at the interphase are not perfect and can be the precursor for damage initiation and propagation.

Although recent research has shown that the interphase plays a critical role in the performance of PMCs, accurate modeling of the interphase is challenging due to the small scale of this region. Reifsnider [10] conducted a parametric study using interphase

* Corresponding author.
E-mail address: Joel.Johnston@asu.edu (J.P. Johnston).

http://dx.doi.org/10.1016/j.compositesb.2016.12.008
1359-8368/

tensile strength as a variable within micromechanical models to investigate the effect on the strength and life of unidirectional composites. Asp et al. [11] assumed symmetrical and periodic conditions in FEA to model a quarter of the fiber in polymer matrix and studied the effects of interphase thickness on the response through a parametric study of various interphase properties. Souza et al. [12] developed a multiscale FEA model incorporating viscoelasticity in the micromechanics and a cohesive zone law representing the interphase to determine the effect of damage under impact loading. FEA has also been used to model representative volume elements (RVEs) consisting of multiple fibers with the interphase represented using bilinear cohesive laws [13,14]. Similar types of interfacial laws have been applied to subcell boundary conditions in the Method of Cells (MOC) [15,16] and the GMC [17–19] theories. Although these studies have applied interfacial laws to account for the fiber/matrix interaction, these microscale interfacial laws are based on larger scale coupon testing or deductions and assumptions from parametric studies.

Due to current limitations in experimental techniques, it is difficult to measure/observe the behavior and failure of the interphase at the atomic/molecular scale. Various test methods have been developed which use single fiber specimens to measure the fiber/polymer interphase strength [20]. One such method called the Broutman test was originally designed to measure the interphase transverse tensile strength for glass fiber PMCs [21] but has also been extended to carbon fiber PMCs [22]. However, this method calculates the transverse tensile strength using the difference in Poisson ratios between the fiber and polymer matrix under a compressive loading condition, and the transverse modulus cannot be measured from this test. While these experimental studies are capable of estimating the interphase properties, the techniques are based on indirect calculation of the properties and thus cannot capture the full range of material properties required to incorporate the interphase within a multiscale analysis.

In order to overcome the nanoscale experimental limitations, a significant amount of modeling research has been reported to study the molecular scale properties of composites using ab-initio quantum chemistry, density functional theory (DFT), and molecular dynamics (MD) methods [23–30]. MD generated properties of graphene nanoplatelets in epoxy were integrated within a multiscale model using GMC micromechanics by Hadden et al. [23]. Jiang et al. [24,25] modeled the macroscopic behavior of CNT-reinforced nanocomposites using a form of the rule of mixtures. In their work, the interphase between the polymer matrix and a CNT is modeled as a wavy surface and a cohesive stress law is formulated based on the Lennard-Jones potential. Mousavi et al. [26] studied the elastic regime of CNT/polymer composites by using a coarse-grained model, which allowed the scaling of cross-linking and molecular interactions to larger length scales. Using these molecular modeling methods, carbon fiber is often approximated as graphene or carbon nanotube (CNT) in order to reduce the number of atoms needed to fully represent the fiber. Zhang et al. [14] estimated the mechanical properties of a carbon fiber/polymer interphase by representing the fiber as multiple layers of graphene and constructing a cohesive law using the van der Waals interactions between the constituents. A vast majority of these molecular interphase models are formulated using only the Lennard-Jones potential, which does not account for mechanical entanglements or covalent bond breakage within the constituents. Additionally, graphene and CNTs possess crystalline structures, whereas carbon fiber is semi-crystalline with chains of carbon atoms randomly folded and/or interlocked together which create defects in the structure [31–34]. Due to the complexity of the carbon fiber, CNT and graphene molecular models cannot be directly applied to simulate the carbon fiber or the fiber interphase.

The focus of this study is to develop a realistic molecular interphase model and integrate it within a multiscale modeling framework. The novel molecular interphase model accounts for structural variation and physical entanglement between the carbon fiber surface and polymer matrix by introducing voids in the graphene layers. A numerical epoxy curing process, previously implemented by the coauthors [35], is applied to the thermoset polymer constituent. The curing process, combined with the semi-crystalline carbon fiber surface, allows the generation and entanglement of polymer chains through the voids of the graphene layers. Several configurations of the interphase model are discussed which include variations in the boundary conditions and structure of the interphase. Virtual transverse tensile tests are performed using the interphase models and the mechanical properties estimated from the results are integrated with the High Fidelity Generalized Method of Cells (HFGMC) theory [36,37], for larger length scale analyses. Multiscale failure and microdamage theories, previously applied to a sectional micromechanics approach by the authors [38,39], are implemented to the current modeling framework. The interphase properties predicted by the current atomistically informed multiscale framework are compared to those obtained from several available studies [11,13,14].

2. Nanoscale constituent models

2.1. Polymer matrix model

In this study, an epoxy-based thermoset polymer consisting of DGEBF resin and Di-Ethylene Tri-Amine (DETA) hardener is simulated in the interphase model using a cut-off distance based covalent bond generation method, which was previously developed by the coauthors for a neat epoxy system [35]. MD simulations are performed using the Large-scale Atomic Molecular Massively Parallel Simulator (LAMMPS) [40] with an all-atom force field called the Merck Molecular Force Field (MMFF) [41]. Information of the MMFF is generated by the Swiss Institute of Bioinformatics [42]. A resin to hardener weight ratio of 100:27 (DGEBF: DETA) is specified by the manufacturer and used to determine the number of molecules for the polymer unit cell (Table 1). Fig. 1 shows a schematic of the 3D molecular structure of neat epoxy where the resin and hardener molecule structures are represented in the dotted boxes.

Table 1
Neat resin components.

	Weight	Formula	# of molecules
DGEBF	313 g/mol	$C_{19}H_{20}O_4$	260
DETA	103 g/mol	$C_4H_{13}N_3$	220

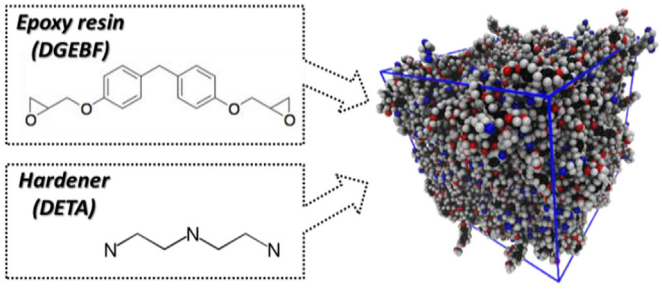

Fig. 1. Schematic of neat epoxy unit cell.

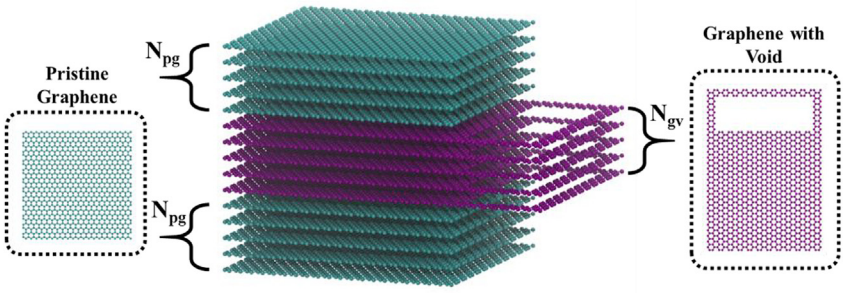

Fig. 2. Molecular representation of the carbon fiber surface using a number of PG layers (N_{pg}) and a number of GV layers (N_{gv}).

2.2. Carbon fiber surface model

The molecular interphase model replicates the semi-crystalline structure of the carbon fiber surface by intentionally creating voids in several protruded graphene layers. The larger size of the protruded, center graphene layers effectively increases the surface roughness of the carbon fiber, thereby simulating a more realistic structure and providing a method to vary the geometry of the structure. Similar processes for defect creation have been applied to CNT models in multiscale FEA analyses [43]. The carbon fiber surface model is constructed by stacking a number of pristine graphene (PG) layers (N_{pg}) and the graphene with void (GV) layers (N_{gv}); a N_{pg}:N_{gv}:N_{pg} (5:5:5) stacking sequence is used as shown in the schematic in Fig. 2. For graphene layers, an all-atom force field is implemented using the Optimized Potential for Liquid Simulation (OPLS) potential to characterize the atomic and molecular interactions [44].

3. Interphase models

The individual constituent models are combined to create a molecular interphase model where the graphene layers and polymer matrix are depicted in the left and right sides of Fig. 3(a), respectively. The numerical curing of the resin and hardener and the simulation of a void in the carbon fiber constituent allows the polymer network to form through the void, which causes entanglement between the carbon fiber surface and the polymer matrix. Due to the entanglement of polymer chains with the GV layers, a large amount of energy is required to break these bonds compared to the non-bonded interactions simulated by the Lennard-Jones potential energy. In order to illustrate the effect of the physical entanglement on the mechanical properties, a variation of the interphase model was developed by replacing the center layers with PG layers which is referred to as the PG interphase model. The initial dimensions of the interphase model are 100 × 65 × 50 $Å^3$, containing 15,000 atoms in the polymer matrix and 15,840 atoms in the carbon fiber surface. As shown in Fig. 3(b), periodic boundary conditions are applied along the y- and z-directions. Energy minimization of the interphase model is performed using the conjugate gradient method. Subsequently, NPT (isobaric-isothermal) ensemble equilibration is performed at 300 K and 1 atm for 10 ns (1 fs time step) using the Nose-Hoover thermostat and barostat. During the 10 ns NPT simulation, the potential energy of the interphase model converges to a mean value with minimal variance which is considered to be the initial, equilibrated state. The cut-off distance based covalent bond generation method is applied to the equilibrated model to generate covalent bonds between the carbon atoms in the resin and the nitrogen atoms in the hardener (C-N bond). The defined cut-off distance is 4 Å, which is approximately the sum of the van der Waals radii of C and N.

To ensure stability in the numerically cured interphase model, additional NPT ensemble simulations (300 K and 1 atm) are performed until the total energy converges to a stable value. Since the classical all-atom force fields, used for the numerical curing process, cannot capture inelastic behavior (bond breakage) of the molecular model, a bond-order based force field is introduced in the equilibrated model to capture covalent bond breakage during the virtual tensile test. The bond-order based force field (also called the reactive force field) developed by Singh et al. [45] is used in this work due to its strong compatibility with hydrocarbon materials. Virtual testing of the interphase model is performed using MD simulations incorporating this force field. It is important to note

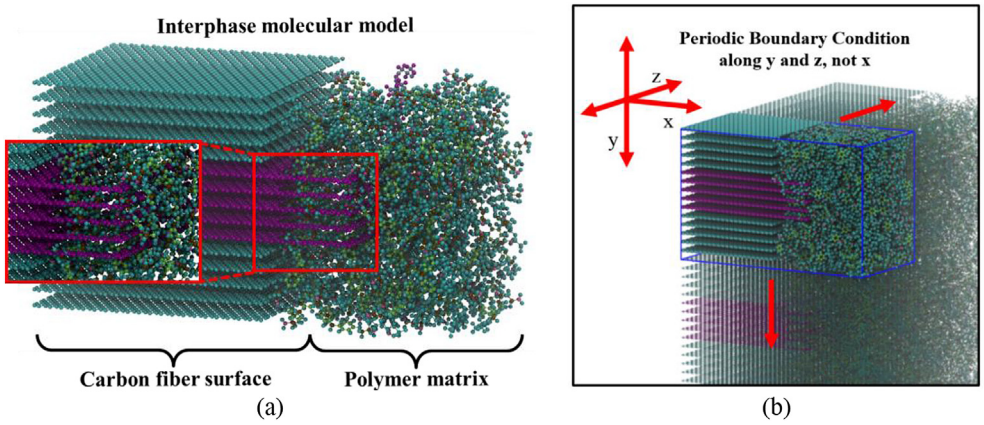

Fig. 3. (a) Molecular structure and (b) periodic boundary conditions of the interphase model.

that the reason for not using the bond-order based force field for the numerical curing and equilibration is because of the computational intensity of this approach. Fig. 4 illustrates the loading conditions for the virtual transverse tensile test where the graphene layers are constrained by a roller joint condition, as shown by the black dotted box, which allows movement only in the y- and z-directions. The red dotted box indicates the displacement condition which is applied to the polymer matrix along the x-axis by displacing either all or half of the polymer atoms as shown in Fig. 4. Fig. 5 shows the boundary and loading conditions for the PG interphase model. The molecular interphase models with the GV layers account for the effects of structural variation and defects on the mechanical properties, whereas the interphase model with only PG layers is used to study the effect of structural variation. Virtual tests are conducted using these models to obtain MD generated elastic and failure properties of the interphase, which are then used in the high fidelity micromechanics theory presented in Section 4.

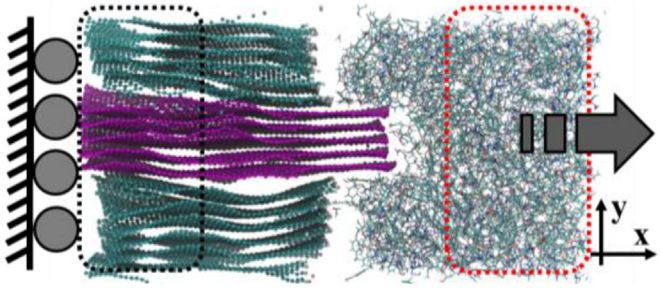

Fig. 5. Schematic of loading conditions for the virtual tensile test of the interphase model with only PG layers.

4. Micromechanical modeling

The HFGMC micromechanics theory [36,37] is employed in the multiscale modeling framework. The micromechanical theory assumes that the composite microstructure is ordered and can be represented by a repeating unit cell consisting of a single fiber in polymer matrix. The unit cell is assumed to be periodically distributed in a space defined by a global coordinate system as illustrated in Fig. 6. A discretization method is used to divide the unit cell into an arbitrary number of rectangular subvolumes called subcells where each subcell can contain a distinct set of material properties.

Since the composite unit cell is defined by a continuous carbon fiber, the computational costs of the microscale simulations are reduced by setting the unit cell thickness in the y_1 direction to be one subcell thick. The interphase subcells are created by replacing the polymer subcells that are immediately adjacent to the fiber subcells as illustrated in Fig. 7. A unit cell discretized into 256 subcells is shown as an example, and a convergence study is described in the results in Section 5.2, which determines the appropriate number of subcells needed to represent the unit cell. The HFGMC theory enables shear coupling between the subcells through the application of a higher order displacement field, which can accurately capture the effect of the interphase on the composite response and failure. The displacement field for each subcell is solved through the assignment of equilibrium, boundary conditions, and interfacial continuity conditions, and the derivation as well as the solution procedure are detailed by Aboudi et al. [36,37]. The properties determined from the nanoscale MD simulations of the interphase are incorporated into the HFGMC micromechanics approach to obtain the unit cell response of the composite.

The constitutive equations for the fiber subcells are defined with a transversely isotropic, linear elastic constitutive law (Equation (1)). The polymer subcells are represented by a modified Bodner-Partom viscoplastic state variable model [46,47] described by Equations (2) and (3), and incorporated within the constitutive law in Equation (4).

$$d\varepsilon_i^f = S_{ij}^f d\sigma_j^f \quad i,j = 1\cdots 6 \tag{1}$$

$$\dot{\varepsilon}_{ij}^I = 2D_0 \exp\left[-\frac{1}{2}\left(\frac{Z}{\sigma_e}\right)^{2n}\right]\left(\frac{\sigma_{ij}^{dev}}{2\sqrt{J_2}} + \alpha\delta_{ij}\right) \quad i,j = 1\cdots 3 \tag{2}$$

$$\sigma_e = \sqrt{3J_2} + \sqrt{3}\alpha\sigma_{kk} \tag{3}$$

$$d\varepsilon_i^m = S_{ij}^m d\sigma_j^m + d\varepsilon_i^I \quad i,j = 1\cdots 6 \tag{4}$$

In Equation (1), the variables $d\varepsilon^f$ and $d\sigma^f$ represent the strain and stress increments of the fiber subcells, respectively, and S^f contains the components of the compliance matrix for the fiber subcells. In Equations (2) and (3), Z and α are variables related to resistance of molecular flow and the hydrostatic stress effects, respectively, D_0 is the maximum inelastic strain rate, and the variable n controls the material rate dependency. The σ^{dev} tensor contains the deviatoric stress components, J_2 is the second invariant of the deviatoric stress tensor, and σ_{kk} is the summation of normal stress components. The variables $d\varepsilon^m$ and $d\sigma^m$ represent the strain and stress increments of the polymer matrix subcells, respectively, and S^m contains the components of the compliance matrix for the polymer matrix subcells. de^I is the inelastic strain increment of the polymer matrix subcells, which is obtained through explicit solutions and converted from matrix notation to Voigt notation. A linear elastic model is used in the interphase subcells and the constitutive equations are similar to that of the fiber subcells described in Equation (1). For the interphase properties obtained from previous

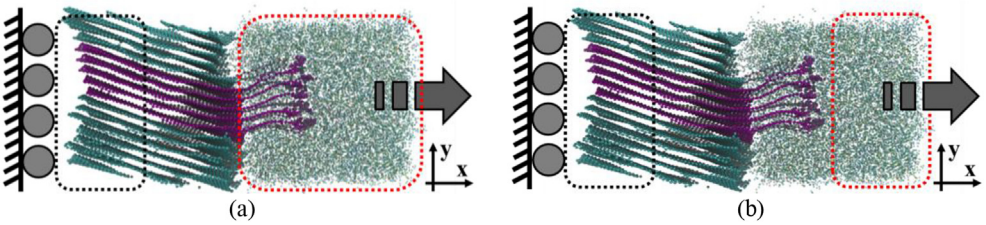

Fig. 4. Boundary conditions for the virtual tensile tests of the interphase model with GV layers where the displacement condition is applied to (a) all the polymer atoms and (b) half of the polymer atoms.

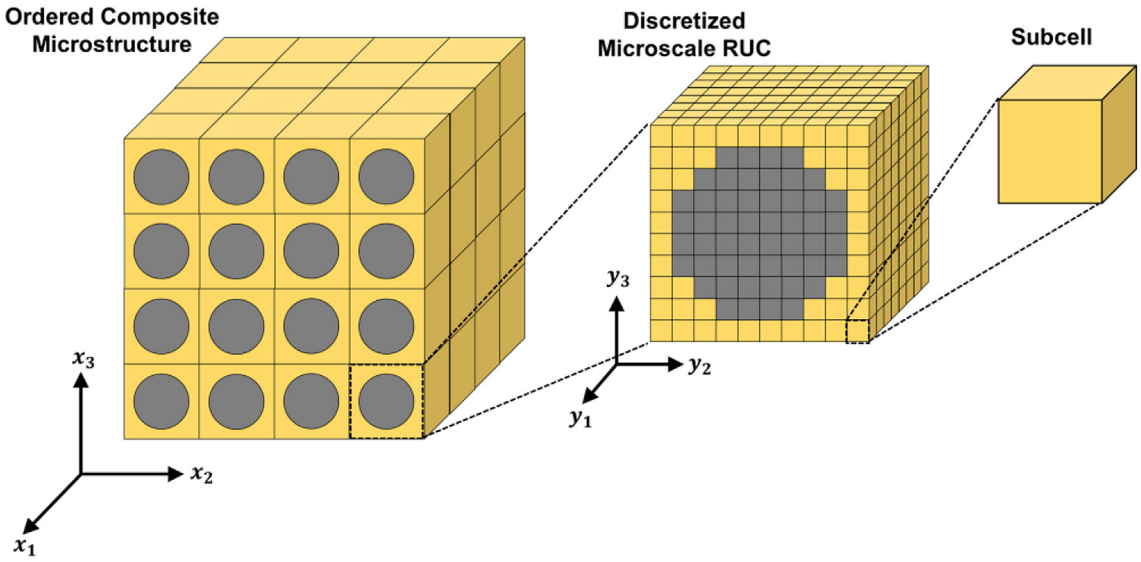

Fig. 6. Schematic showing the discretization process of a fiber PMC microstructure.

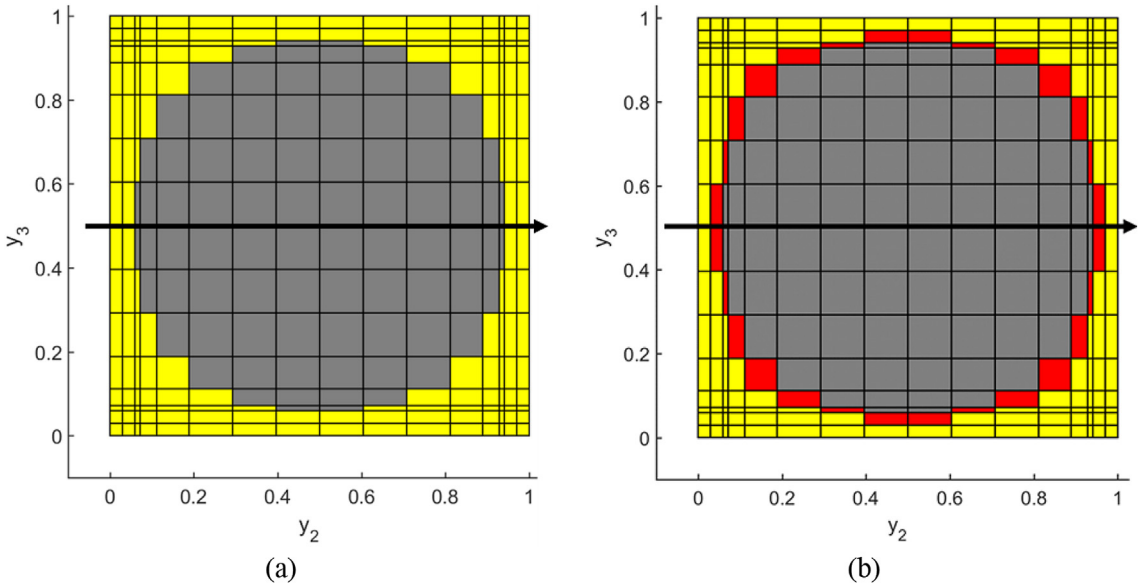

Fig. 7. Discretization of a microscale unit cell (a) without an interphase and (b) with an interphase into polymer (yellow), fiber (grey), and interphase (red) subcells. (For interpretation of the references to colour in this figure legend, the reader is referred to the web version of this article.)

studies, the material symmetry of the interphase is defined as either isotropic or transversely isotropic based on the assumptions outlined in the respective studies.

In the current model, damage and failure criteria are applied to the subcells and the unit cell. Progressive damage is modeled using a work potential theory [48], which can capture microscale damage by discretizing the strain energy into elastic and damage components. The work potential theory has been integrated into the GMC theory through a progressive damage model with plane stress conditions [49,50]. A 3D form of this progressive damage theory was incorporated in a sectional micromechanical model [38,39] by the authors. This damage theory is applied to the 3D constitutive law of the polymer subcells where the damage parameters, calculated at each time step, degrade the elastic modulus of the polymer. The microscale failure modes of the polymer and interphase subcells are determined through a maximum strain criterion and maximum stress criterion, respectively. The maximum strain criterion is used for the polymer subcells due to the highly nonlinear response caused by the viscoplastic behavior of the polymer. The macroscale failure criteria of the unit cell is based on a modified Hashin failure theory that incorporates shear stress terms in the compressive fiber failure mode [51,52].

5. Results and discussion

5.1. Molecular interphase results

The nanoscale properties of the interphase are estimated through the virtual tensile testing of the atomistic interphase model. Deformation is applied to the polymer matrix at a constant

rate of 0.001 Å/fs (displacement condition) with the previously described boundary conditions. High displacement rates are needed in MD simulations in order to account for molecular interactions. However, the total time of the simulations with these high displacement rates is constrained to a few nanoseconds due to computational limitations. Fig. 8(a) and (b) show how the different displacement configurations affect the straining of the GV layers and polymer matrix, and that the GV interphase model configuration displacing half the polymer atoms depicts a more accurate representation of the physical loading mechanisms in the material. The simulation results (Fig. 8c) of the PG interphase demonstrate straining of only the polymer matrix. Additionally, the polymer atoms near the protruded graphene layers in the PG interphase results show less deformation compared to the polymer atoms away from the graphene layers; this shows the effect of structural variation on the material response. Fig. 8 shows the stress-strain plots of the MD simulations based on the spatially and temporally averaged virial stress calculation [53]. The results show that displacing all the polymer atoms in the GV interphase model yields minimal straining of the polymer matrix molecules resulting in a high stress concentration at the carbon chains around the void and lower failure strain of 5%. By displacing half of the polymer atoms in the GV interphase, the polymer matrix molecules in the void and adjacent to the carbon fiber surface are strained, which relieves the stress concentration and causes a decrease in stiffness. The stress-strain results for the PG interphase

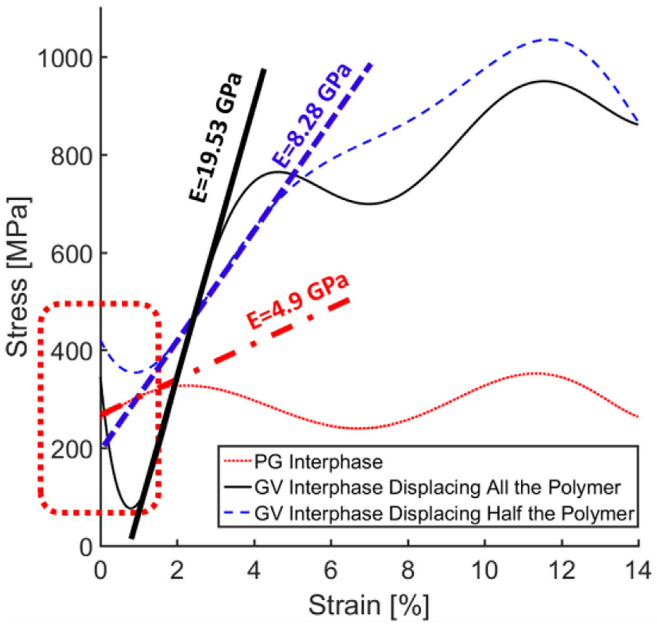

Fig. 9. Stress-strain plots from the virtual test results of the interphase models.

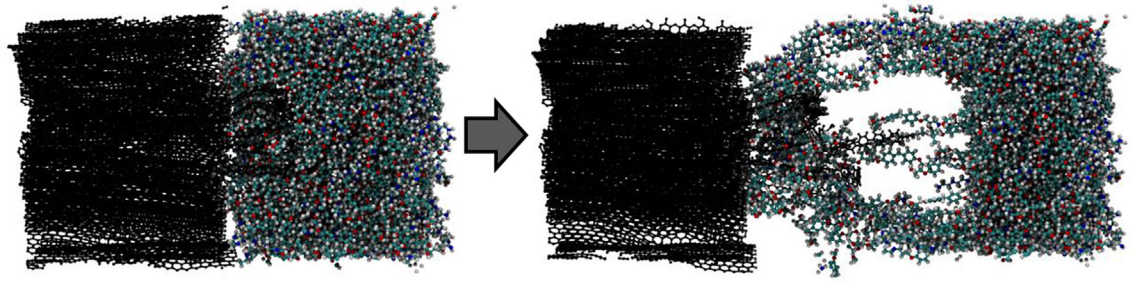

(a) Graphene with void (GV) interphase model displacing half the polymer

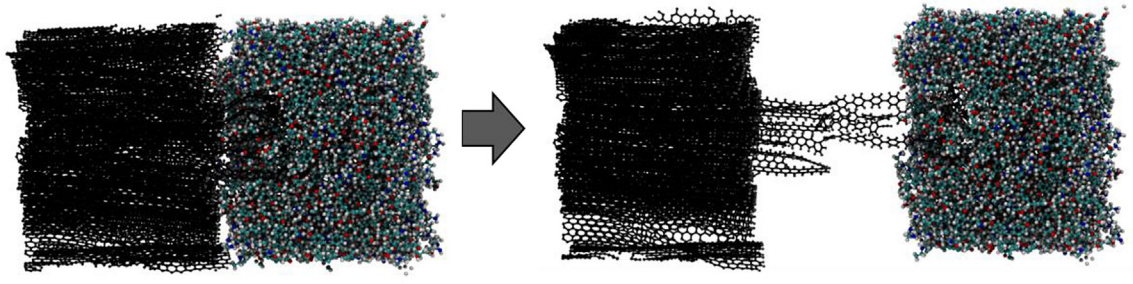

(b) Graphene with void (GV) interphase model displacing all the polymer

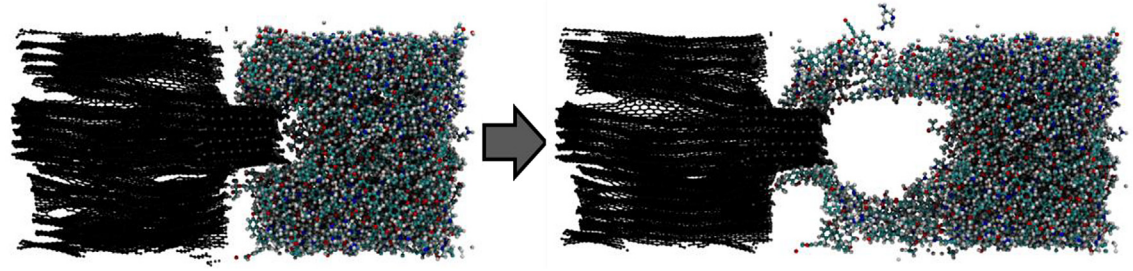

(c) Pristine graphene (PG) interphase model

Fig. 8. Virtual test results of the equilibrated molecular interphase models showing the position of the atoms before (left) and after (right) testing.

Table 2
Interphase material properties.

	Transverse modulus (GPa)	Transverse tensile strength (MPa)
Wang et al. [13]	12.7	50
Zhang et al. [14]	3.37	53
Asp et al. [11]	34	50[a]
Current Model – GV Displacing All the Polymer	19.53	783.5
Current Model – GV Displacing Half the Polymer	8.28	1024
Current Model – PG	4.9	377.5

[a] Value assumed; not available in reference.

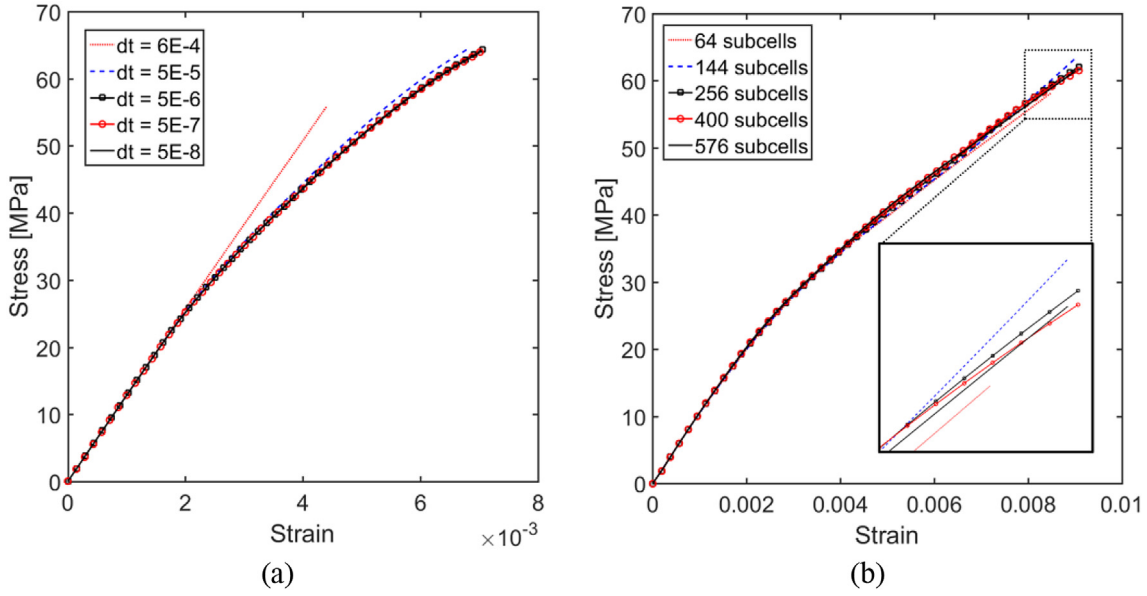

Fig. 10. Micromechanics convergence study of (a) the time increment and (b) the number of subcells.

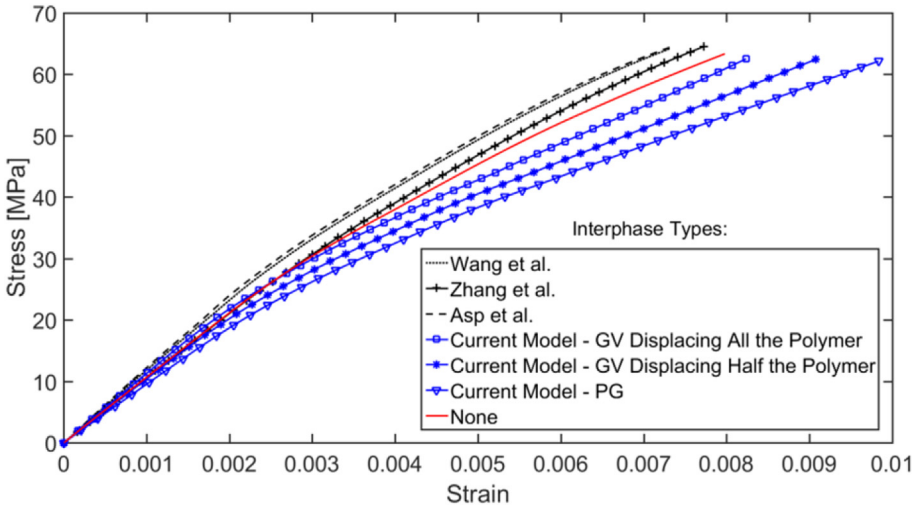

Fig. 11. Transverse tensile stress-strain plots for unit cells with different interphase properties.

model produce low stiffness and failure values indicating a dependence on the Lennard-Jones potential due to the void-free structure of the model which prevents entanglement between the carbon fiber surface and the polymer matrix. The dotted red box in Fig. 9 shows irregularities at the initial stage of the stress-strain plots, which are caused by a temporary lack of contact between the carbon fiber surface and the polymer matrix. Additionally, due to the potential energy caused by the formation of bonded and non-bonded interactions during the equilibration simulation, the stress-strain plots have an initial stress value.

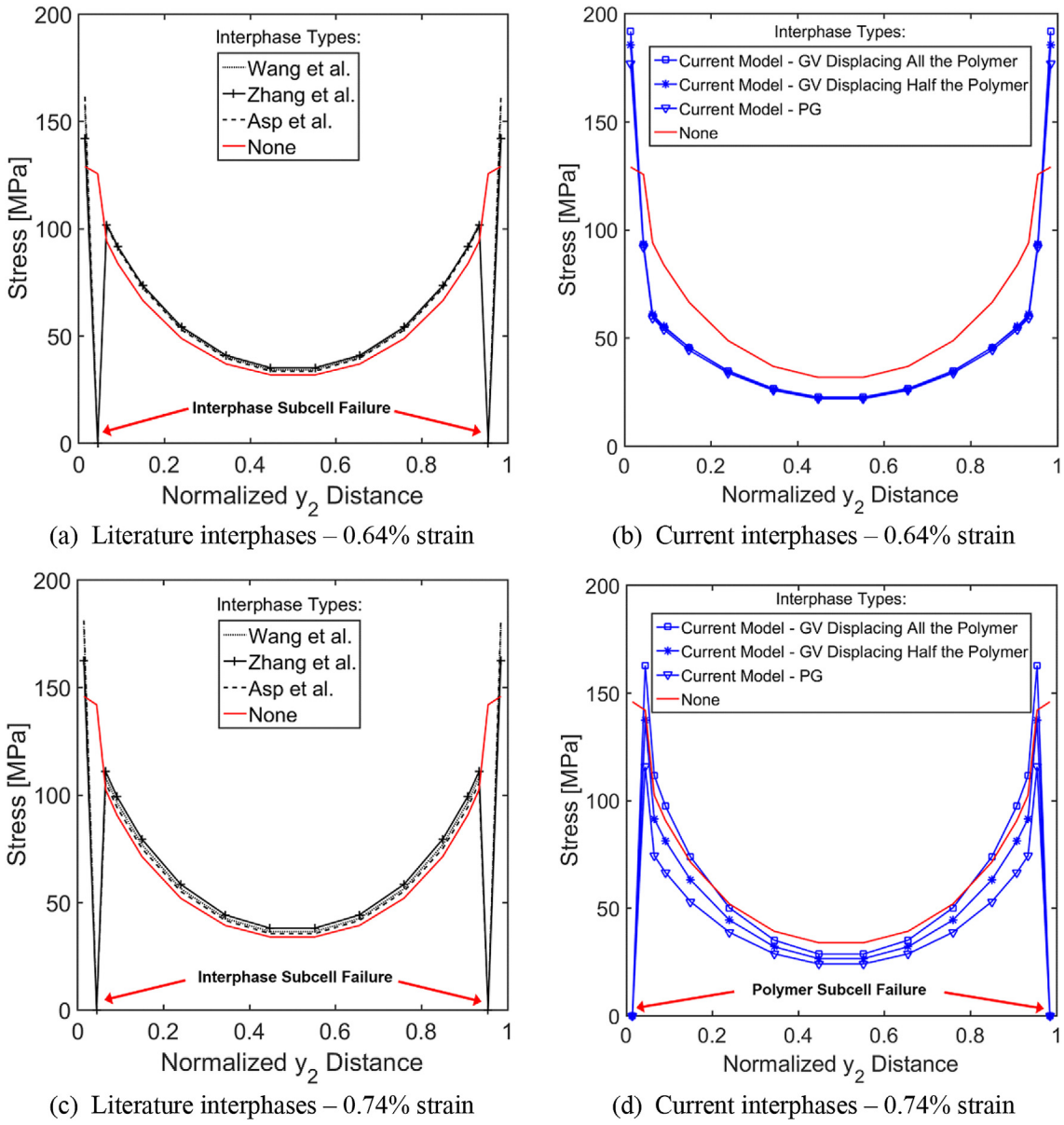

Fig. 12. Subcell stress-width plots for unit cell simulations.

Therefore, the portion of the stress-strain curve ranging from 1% to 3% strain is used to calculate the transverse moduli.

5.2. High fidelity micromechanics results

Various interphase properties from the literature are investigated using the micromechanics technique to compare with those obtained using the MD simulated properties. Table 2 displays the transverse properties for each interphase type including the current MD simulated properties. The first interphase type refers to the properties obtained by Wang et al. [13] using dynamic modulus imaging methods. The interphase properties from Zhang et al. [14] are calculated using a cohesive law derived from the Lennard-Jones potential and they applied factors to capture microscopic defects. The final literature interphase uses an intermediate modulus from a parametric study performed by Asp et al. [11]. A difference in strength values between the current model and literature values is evident because the values from literature are computed based on models or analytical techniques that only consider the Lennard-Jones potential. The transverse tensile modeling results are obtained by applying a strain rate of 1.05 s^{-1} to the PMC microscale unit cell.

A convergence study is performed to determine an appropriate time increment and a sufficient number of subcells required for the micromechanics simulations. The GV interphase model with half the polymer atoms being displaced was used in this convergence study. The stress-strain responses of the unit cell, for various time increments, are shown in Fig. 10(a) and convergence of the response, including failure, is achieved with a time increment of 5E-6. The convergence study for the number of subcells is presented in Fig. 10(b) and shows that the unit cell stress-strain response converges with a simulation containing 256 subcells. The converged parameters are used in the subsequent simulations to compare the different interphase models and properties.

Transverse tensile stress-strain plots of unit cell simulations with different interphase types are depicted in Fig. 11. For comparison, these results are plotted with simulation results obtained from a unit cell without interphase subcells. The stress-strain

response for the simulations with interphase properties from literature (Table 2) shows smaller failure strains compared to the simulation without interphase subcells. In contrast, the simulations with the current interphase models result in a 5% lower transverse tensile strength and increased nonlinearity causing 25% larger failure strains. To plot the transverse tensile stress as a function of normalized unit cell width, subcell stress values are extracted as shown by the arrow bisecting the unit cell in the y_2 direction in Fig. 7. The subcell stress-width data for the simulations with the interphase types from literature, presented in Fig. 12(c), shows local failure of the interphase subcells. In contrast, Fig. 12(d) demonstrates that local failure in the unit cell simulation results, obtained using the current interphase models, occurs in the polymer subcells. Additionally, the simulations with the current interphase models show a larger stress gradient across the interphase due to the properties and material symmetry applied to these models (Fig. 12a and b). The large stress gradients and local failure modes increase the viscoplastic straining of the polymer subcells, which causes the large nonlinearity in the unit cell simulations with the current interphase models. It is important to note that the large variations in transverse elastic moduli of different interphase types does not affect the mode of local failure, whereas the interphase strength and structure does affect the mode of local failure.

Similar results were obtained in Maligno et al. [54] where a finite element model of a composite RVE was simulated and parametric studies were performed using interphase strength as a variable. For interphase strengths less than about 60 MPa, Maligno's results showed that local failure initiated in the interphase elements and, for higher values of interphase strengths, local failure occurred in the polymer elements. These results were obtained using varying interphase transverse elastic moduli and the moduli variations did not have an effect on the mode of local failure which agrees with the results from the current simulations.

6. Concluding remarks

This study uses a nanoscale interphase model composed of multiple GV layers and a thermoset polymer matrix to represent the physical molecular structure of the interphase. The GV layers were created by removing carbon atoms which caused voids in the layers. The results from the MD simulations show that strong carbon fiber/polymer matrix interactions exist in the GV interphase models yielding larger stiffness and strength compared to the PG interphase model. A multiscale framework was developed to integrate the interphase models with a high fidelity micromechanics theory. The complex interactions shown in the MD results, due to voids and structural variation, cause large stress gradients across the interphase and increased viscoplastic behaviour in the microscale simulations. A comparison of the microscale results showed that the unit cell response obtained using the current interphase model predict a slightly lower composite tensile strength (about 5%) and a maximum difference of 25% in failure strain compared to the results obtained using interphase properties from the literature.

Acknowledgements

This research is supported by the U.S. Army Research Office, grant number: W911NF-15-1-0072, technical monitor: Dr. David Stepp.

References

[1] Voyiadjis GZ, Deliktas B, Aifantis EC. Multiscale analysis of multiple damage mechanisms coupled with inelastic behavior of composite materials. J Eng Mech 2001;127:636–45.
[2] Yu Q, Fish J. Multiscale asymptotic homogenization for multiphysics problems with multiple spatial and temporal scales: a coupled thermo-viscoelastic example problem. Int J Sol Struct 2002;39:6429–52. http://dx.doi.org/10.1016/S0020-7683(02)00255-X.
[3] Bednarcyk BA, Arnold SM. In: A framework for performing multiscale stochastic progressive failure analysis of composite structures; 2007. Boston, MA, United States.
[4] Liu KC, Chattopadhyay A, Bednarcyk BA, Arnold SM. Efficient multiscale modeling framework for triaxially braided composites using generalized method of cells. J Aerosp Eng 2011;24:162–9. http://dx.doi.org/10.1061/(ASCE)AS.1943-5525.0000009.
[5] Liu KC. Micromechanics based multiscale modeling of the inelastic response and failure of complex architecture composites. Arizona State University; 2011.
[6] Laurin F, Carrère N, Maire J-F. A multiscale progressive failure approach for composite laminates based on thermodynamical viscoelastic and damage models. Compos Part A Appl Sci Manuf 2007;38:198–209. http://dx.doi.org/10.1016/j.compositesa.2006.01.018.
[7] Ghosh S, Lee K, Raghavan P. A multi-level computational model for multi-scale damage analysis in composite and porous materials. Int J Sol Struct 2001;38:2335–85. http://dx.doi.org/10.1016/S0020-7683(00)00167-0.
[8] Ghosh S, Lee K, Moorthy S. Multiple scale analysis of heterogeneous elastic structures using homogenization theory and voronoi cell finite element method. Int J Sol Struct 1995;32:27–62. http://dx.doi.org/10.1016/0020-7683(94)00097-G.
[9] Borkowski LB, Liu KC, Chattopadhyay A. From ordered to disordered: the effect of microstructure on composite mechanical performance. CMC Comput Mater Contin 2013;37:161–93.
[10] Reifsnider KL. Modelling of the interphase in polymer-matrix composite material systems. Composites 1994;25:461–9. http://dx.doi.org/10.1016/0010-4361(94)90170-8.
[11] Asp LE, Berglund LA, Talreja R. Effects of fiber and interphase on matrix-initiated transverse failure in polymer composites. Compos Sci Technol 1996;56:657–65. http://dx.doi.org/10.1016/0266-3538(96)00047-4.
[12] Souza FV, Allen DH, Kim Y-R. Multiscale model for predicting damage evolution in composites due to impact loading. Compos Sci Technol 2008;68:2624–34. http://dx.doi.org/10.1016/j.compscitech.2008.04.043.
[13] Wang X, Zhang J, Wang Z, Zhou S, Sun X. Effects of interphase properties in unidirectional fiber reinforced composite materials. Mater Des 2011;32:3486–92. http://dx.doi.org/10.1016/j.matdes.2011.01.029.
[14] Zhang B, Yang Z, Sun X, Tang Z. A virtual experimental approach to estimate composite mechanical properties: modeling with an explicit finite element method. Comput Mater Sci 2010;49:645–51. http://dx.doi.org/10.1016/j.commatsci.2010.06.007.
[15] Aboudi J. Damage in composites—modeling of imperfect bonding. Compos Sci Technol 1987;28:103–28.
[16] Aboudi J. Constitutive equations for elastoplastic composites with imperfect bonding. Int J Plati 1988;4:103–25. http://dx.doi.org/10.1016/0749-6419(88)90016-2.
[17] Bednarcyk BA, Arnold SM. MAC/GMC 4.0 User's manual volume 3: example manual. 2002. NASA Technical Memorandum. 212077.
[18] Goldberg RK, Arnold SM. A study of influencing factors on the tensile response of a titanium matrix composite with weak interfacial bonding. 2000.
[19] Aboudi J. Constitutive behavior of multiphase metal matrix composites with interfacial damage by the generalized cells model. Stud Appl Mech 1993;34:3.3.
[20] Zhandarov S, Mäder E. Characterization of fiber/matrix interface strength: applicability of different tests, approaches and parameters. Compos Sci Technol 2005;65:149–60. http://dx.doi.org/10.1016/j.compscitech.2004.07.003.
[21] Broutman L. Measurement of the fiber-polymer matrix interfacial strength. In: Interfaces in composites. ASTM International; 1969.
[22] Ageorges C, Friedrich K, Ye L. Experiments to relate carbon-fibre surface treatments to composite mechanical properties. Compos Sci Technol 1999;59:2101–13. http://dx.doi.org/10.1016/S0266-3538(99)00067-6.
[23] Hadden CM, Klimek-McDonald DR, Pineda EJ, King JA, Reichanadter AM, Miskioglu I, et al. Mechanical properties of graphene nanoplatelet/carbon fiber/epoxy hybrid composites: multiscale modeling and experiments. Carbon 2015;95:100–12. http://dx.doi.org/10.1016/j.carbon.2015.08.026.
[24] Jiang L, Tan H, Wu J, Huang Y, Hwang K-C. Continuum modeling of interfaces in polymer matrix composites reinforced by carbon nanotubes. Nano 2007;2:139–48. http://dx.doi.org/10.1142/S1793292007000519.
[25] Jiang L. Development of an enhanced microstructure–level machining model for carbon nanotube reinforced polymer composites using cohesive zone interface. University of Illinois at Urbana–Champaign; 2013.
[26] Mousavi AA, Arash B, Zhuang X, Rabczuk T. A coarse-grained model for the elastic properties of cross linked short carbon nanotube/polymer composites. Compos Part B: Eng 2016;95:404–11. http://dx.doi.org/10.1016/j.compositesb.2016.03.044.
[27] Shiu S-C, Tsai J-L. Characterizing thermal and mechanical properties of graphene/epoxy nanocomposites. Compos Part B Eng 2014;56:691–7. http://dx.doi.org/10.1016/j.compositesb.2013.09.007.
[28] Shin H, Chang S, Yang S, Youn BD, Cho M. Statistical multiscale homogenization approach for analyzing polymer nanocomposites that include model inherent uncertainties of molecular dynamics simulations. Compos Part B Eng

2016;87:120–31. http://dx.doi.org/10.1016/j.compositesb.2015.09.043.
[29] Rahman R, Haque A. Molecular modeling of crosslinked graphene–epoxy nanocomposites for characterization of elastic constants and interfacial properties. Compos Part B Eng 2013;54:353–64. http://dx.doi.org/10.1016/j.compositesb.2013.05.034.
[30] Ionita M. Multiscale molecular modeling of SWCNTs/epoxy resin composites mechanical behaviour. Compos Part B Eng 2012;43:3491–6. http://dx.doi.org/10.1016/j.compositesb.2011.12.008.
[31] Edwards IA, Menendez R, Marsh H. Introduction to carbon science. Butterworth-Heinemann; 2013.
[32] Johnson DJ. Structure-property relationships in carbon fibres. J Phys D: Appl Phys 1987;20:286. http://dx.doi.org/10.1088/0022-3727/20/3/007.
[33] Guigon M, Oberlin A. Heat-treatment of high tensile strength PAN-based carbon fibres: microtexture, structure and mechanical properties. Compos Sci Technol 1986;27:1–23. http://dx.doi.org/10.1016/0266-3538(86)90060-6.
[34] Zhang Y, Xu F, Zhang C, Wang J, Jia Z, Hui D, et al. Tensile and interfacial properties of polyacrylonitrile-based carbon fiber after different cryogenic treated condition. Compos Part B Eng 2016;99:358–65. http://dx.doi.org/10.1016/j.compositesb.2016.05.056.
[35] Koo B, Liu Y, Zou J, Chattopadhyay A, Dai LL. Study of glass transition temperature (T g) of novel stress-sensitive composites using molecular dynamic simulation. Model Simul Mat Sci Eng 2014;22:65018. http://dx.doi.org/10.1088/0965-0393/22/6/065018.
[36] Aboudi J, Pindera M-J, Arnold SM. High-fidelity generalization method of cells for inelastic periodic multiphase materials. 2002. http://ntrs.nasa.gov/search.jsp?R=20020061830 (accessed 2 February, 2016).
[37] Aboudi J, Arnold SM, Bednarcyk BA. Micromechanics of composite materials: a generalized multiscale analysis approach. Butterworth-Heinemann; 2012.
[38] Johnston J, Chattopadhyay A. Effect of material variability on multiscale modeling of rate-dependent composite materials. J Aerosp Eng 2015;28:4015003. http://dx.doi.org/10.1061/(ASCE)AS.1943-5525.0000488.
[39] Johnston J, Heitland C, Chattopadhyay A. Effect of material variability on progressive damage and micromechanics of composite materials. Orlando, Florida, USA: American Institute of Aeronautics and Astronautics; 2015. p. 1.
[40] Plimpton S. Fast Parallel algorithms for short-range molecular dynamics. J Comput Phys 1995;117:1–19. http://dx.doi.org/10.1006/jcph.1995.1039.
[41] Halgren TA. Merck molecular force field. I. Basis, form, scope, parameterization, and performance of MMFF94. J Comput Chem 1996;17:490–519.
[42] Zoete V, Cuendet MA, Grosdidier A, Michielin O. SwissParam: a fast force field generation tool for small organic molecules. J Comput Chem 2011;32:2359–68. http://dx.doi.org/10.1002/jcc.21816.
[43] Gupta AK, Harsha SP. Analysis of mechanical properties of carbon nanotube reinforced polymer composites using multi-scale finite element modeling approach. Compos Part B Eng 2016;95:172–8. http://dx.doi.org/10.1016/j.compositesb.2016.04.005.
[44] Jorgensen WL, Maxwell DS, Tirado-Rives J. Development and testing of the OPLS all-atom force field on conformational energetics and properties of organic liquids. J Am Chem Soc 1996;118:11225–36.
[45] Singh SK, Srinivasan SG, Neek-Amal M, Costamagna S, van Duin AC, Peeters FM. Thermal properties of fluorinated graphene. Phys Rev B 2013;87:104114.
[46] Bodner SR. Unified plasticity for engineering applications. Springer Science & Business Media; 2002.
[47] Goldberg R, Roberts G, Gilat A. Implementation of an associative flow rule including hydrostatic stress effects into the high strain rate deformation analysis of polymer matrix composites. J Aerosp Eng 2005;18:18–27. http://dx.doi.org/10.1061/(ASCE)0893-1321(2005)18:1(18).
[48] Schapery RA. A theory of mechanical behavior of elastic media with growing damage and other changes in structure. J Mech Phys Sol 1990;38:215–53. http://dx.doi.org/10.1016/0022-5096(90)90035-3.
[49] Pineda EJ, Waas AM, Bednarcyk BA, Collier CS, Yarrington PW. Progressive damage and failure modeling in notched laminated fiber reinforced composites. Int J Fract 2009;158:125–43. http://dx.doi.org/10.1007/s10704-009-9370-3.
[50] Pineda EJ. A novel multiscale physics-based progressive damage and failure modeling tool for advanced composite structures. NASA Glenn Research Center; 2012.
[51] Zhu L, Chattopadhyay A, Goldberg RK. Failure model for rate-dependent polymer matrix composite laminates under high-velocity impact. J Aerosp Eng 2008;21:132–9.
[52] Hashin Z. Failure criteria for unidirectional fiber composites. ASME 1980;47:329–34.
[53] Subramaniyan AK, Sun CT. Continuum interpretation of virial stress in molecular simulations. Int J Sol Struct 2008;45:4340–6. http://dx.doi.org/10.1016/j.ijsolstr.2008.03.016.
[54] Maligno AR, Warrior NA, Long AC. Effects of interphase material properties in unidirectional fibre reinforced composites. Compos Sci Technol 2010;70:36–44. http://dx.doi.org/10.1016/j.compscitech.2009.09.003.